A preliminary organic geochemical and petrographical investigation of Neyveli Lignite (Mine–1) to understand the depositional environment and Hydrocarbon Source characteristics

SNEHA SANTHOSH[1], RUNCIE P. MATHEWS[2*], SATENDRA KUMAR GUPTA[2] AND BHAGWAN D. SINGH[2]

[1]*Department of Oceanography, FOST, Kerala University of Fisheries and Ocean Studies, Kochi 682506, India.*
[2]*Birbal Sahni Institute of Palaeosciences, 53 University Road, Lucknow 226 007, India.*
*Corresponding author: rp_mathews@bsip.res.in

ABSTRACT

Sneha S, Mathews RP, Gupta SK & Singh BD 2024. A preliminary organic geochemical and petrographical investigation of Neyveli Lignite (Mine–1) to understand the depositional environment and hydrocarbon source characteristics. Journal of Palaeosciences 73(2): 131–148.

The lignite deposit of Neyveli Mine–1 associated with the Cuddalore Formation (Miocene) of Cauvery Basin, South India is studied using a combination of organic geochemical (FTIR spectroscopy and GC–MS) and organic petrographical analyses to identify the composition and kerogen type to reconstruct its palaeoflora and palaeodepositional setting. Further the thermal maturity attained and hydrocarbon source potential of these organic–rich deposits have also been investigated. The petrographic study shows huminite maceral as the most abundant group with an average of ~78 av. vol.% with subordinate liptinite (avg. ~10 vol.%) and inertinite (avg. ~4 vol.%) composition. The petrographical facies indices (GI–TPI, GWI–VI) indicate a mixed type of organic matter deposited in a limno–telmatic regime under mesotrophic to rheotrophic hydrological conditions. The occurrence of varying hydrological conditions is well supported by the P_{aq} values (0.23–0.32), $Pr/n–C_{17}$ and $Ph/n–C_{18}$ ratios. The presence of ulminite, resinite, sporinite, suberinite and cutinite macerals along with high CPI (avg. 3.16), TAR (avg. 17.27), high P_{wax} ratio (avg. 0.81) and high abundance of long–chain alkanes ($n–C_{27}$ and $n–C_{29}$), supports the presence of higher plants while the microbial degradation of the vegetal debris and/or the presence of herbaceous plants in the source flora is deciphered from the high percentage of detrohuminite (avg. ~55 vol.%). Alginite submaceral suggests algal input further pointing to fresh water/lacustrine conditions in the vicinity. The percentage of funginite (~3 avg. vol.%) and the ACL values (avg. 28.81) represent a warm and humid palaeoclimate. The Pr/Ph ratio and $Pr/n–C_{17}$ vs $Ph/n–C_{18}$ plot indicate the suboxic to anoxic redox conditions (transitional environment). The FTIR spectra showed prominent hydroxyl, aliphatic, aromatic and carboxyl/carbonyl groups typical in organic–rich sedimentary samples. The huminite reflectance suggests a rank of low–rank B (av. 0.37% Rr), suggesting thermal immaturity of the samples. Multiple facies diagrams indicate this lignite possesses admixed type–III/II kerogen which can generate mainly gas and a little oil generation upon maturation.

Key–words—Neyveli Lignite, FTIR, *n*–alkanes, Macerals, Palaeoenvironment, Hydrocarbons..

INTRODUCTION

THE tectono–geomorphic alteration of the Indian subcontinent was initiated approximately 167 million years ago subsequent to the disintegration of the Gondwana supercontinent (Ramkumar *et al.*, 2017). During the northward drift of the Indian subcontinent, it travelled through various climatic zones which resulted in the rapid growth of vegetation (Singh *et al.*, 2022) and also the subcontinent went through several geologic and tectonic evolutions that contributed to the formation of Palaeozoic to Cenozoic sedimentary basins, plateaus, and escarpments (Ramkumar *et al.*, 2017). The South Arcot Basin or Ariyalur–Pondicherry sub–basin of the Cauvery main basin on the East Coast of India contains the

largest exploitable Cenozoic lignite reserve. This reserve is located at Neyveli and its surrounding areas, situated at a latitude of 11°15'–11°40' and a longitude of 79°25'–79°40' (Singh *et al.*, 1992).

The Neyveli Lignite had previously been characterised and investigated by several researchers (Navale, 1967; Navale & Misra, 1980; Misra, 1992; Saxena, 1992; Singh *et al.*, 1992; Singh & Singh, 1994; Singh & Misra, 1999 and many more) to understand its maceral composition, palynology, palaeoecology, palaeodepositional settings, palaeovegetation, palaeoclimate, rank, thermal maturity, age, etc. The available information on the characteristics of Neyveli Lignite is mainly
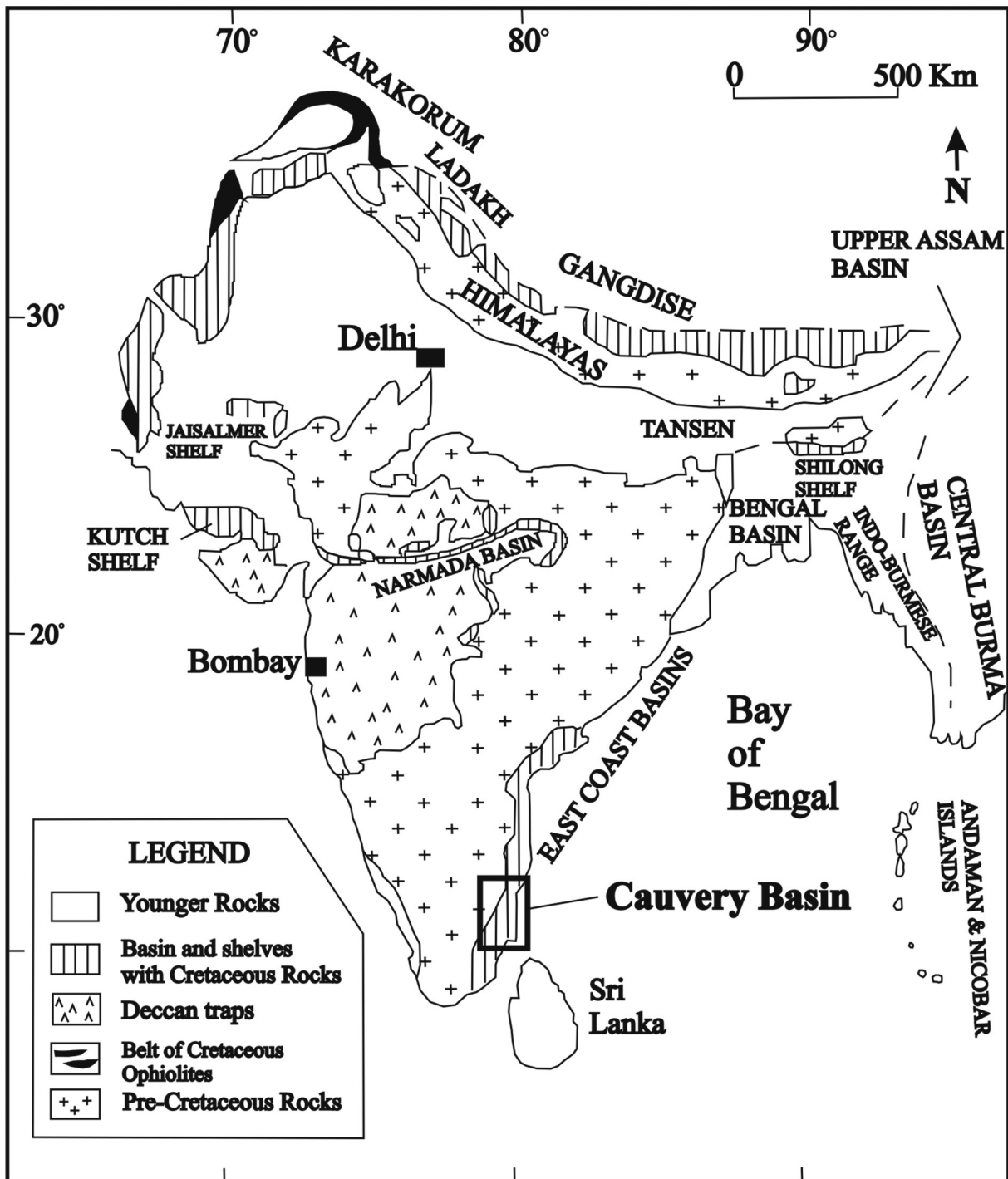

Fig. 1—Indian Sub–Continent highlighting Cauvery Basin (after Watkinson *et al.*, 2007).

based on both incident and fluorescence light microscopic studies. In this study, the lignite samples from Neyveli Mine–1 are characterised using maceral analysis and geochemical techniques such as Fourier Transform Infrared Spectroscopy (FTIR) and Gas Chromatography–Mass Spectrometry (GC–MS) in order to have more comprehensive understanding about the origin and depositional conditions. The organic matter source, palaeodepositional settings and palaeoclimate are determined by organic–geochemical analysis (n–alkane distribution pattern analysis) using GC–MS, whereas the FTIR Spectroscopy is mainly used to determine the organic functional groups present in the samples to understand the kerogen type and hydrocarbon source potential of the Neyveli Lignite. The results obtained from these analyses are combined with the results derived from organic petrographic study to ensure a multiproxy approach to the characterisation of Neyveli Lignite.

The main objectives of this study include the identification of composition and variations of macerals in the Neyveli Lignite, determination of its rank with the help of huminite reflectance measurement, determining the hydrocarbon source potential and type of kerogen through FTIR Spectroscopy and also with the help of maceral compositions obtained by organic petrography. The reconstruction of palaeoflora, palaeodepositional settings, and palaeoclimatic condition is done with the data obtained from organic petrography, FTIR Spectroscopy, and GC–MS analysis.

STUDY AREA

The Cauvery Basin (Fig. 1) is a pericratonic–rift basin (Chakraborty et al., 2010; Nagendra & Reddy, 2017) formed due to the fragmentation of Gondwanaland during the Lower Cretaceous Period (Ramkumar et al., 2011). Within the basin, there are numerous horsts and grabens, and the Lower Cretaceous Andimadam Formation and Sattapadi Shale contain thick organic–rich source rocks (Karthikeyan et al., 2018). It is common to find broad depressions surrounded by narrow ridges in the basin (Chakraborty et al., 2010). The northern part of the basin is marked by the Ariyalur–Pondicherry depression, which is bounded to the southeast by the Kumbakonam–Shyali Ridge. The main central low subparallel to the Ariyalur–Pondicherry depression is Tanjavur and Tranquebar. Further south, there are two depressions, namely Nagipattinam Palk Bay, which are bounded similarly by the Karaikal High and Devakottai–Mannargudi Ridge in the north, and the Vedarnayam High and Mendapam Ridge in the south. The southernmost part of the basin is characterised by the Mannar depression (Sastri et al., 1973; Chakraborty et al., 2010; Premarathne, 2015).

The basement of the Cauvery Basin constitutes igneous and metamorphic complexes of the Archaean age, which are overlain by Sivaganga beds, the Dalmiapuram Formation,

and the upper Cretaceous formations (Sastri et al., 1973). The upper Cretaceous formations are overlained by Pondicherry as well as Niniyur formations which are Palaeocene formations (Sastri et al., 1973; Chari et al., 1995) and the lignite deposits of Neyveli are found at a depth of 45 to 120 m below ground level (Khan et al., 2005) in a stratigraphic sequence of clay, sand, sandstone, and gravel beds belonging to the Cuddalore Series of late Miocene age (Jones & Subramanyam, 1961; Pranesh et al., 2019).

Neyveli Lignite Mine is located in the Cuddalore District, Tamil Nadu, about 200 km to the southern part of Chennai (Periyasamy, 2019). In the year 1956, the Government of India founded Neyveli Lignite Corporation Limited (NLC) for the commercial exploitation of lignite and now it is known as NLC India Ltd. The lignite deposits are present over a vast expanse of 330 km^2 and have an approximate estimated reserve of 3300 MT (source: NLC India Limited). Neyveli Lignite Mine–1 (Fig. 2a) has a lignite production capacity of 10.5 MT per annum.

METHODOLOGY

The samples of Neyveli Lignite (Mine–1) were analysed by using organic petrographic analysis (maceral counting & Huminite reflectance measurement), FTIR Spectroscopy, and Gas Chromatography–Mass Spectrometry. Nine lignite samples from different positions of the seam (Fig. 2b, c) were analysed by FTIR spectroscopy as well as organic petrography and GC–MS study was carried out on 3 representative lignite samples for assessing n–alkane distributions.

Petrographic analysis

The sample preparation, maceral analysis, and measurement of reflectance was carried out according to the ISO 7404–2 (2009), ISO 7404–3 (2009), ISO 7404–5 (2009) rules and regulations, and the ICCP nomenclature. The Leica DM4P microscope was used for the analysis of macerals and measuring huminite (ulminite) reflectance. TIDAS MSP 400 spectrophotometer (CDD UV/NIR) and CoalExpert (1.4.0.6 version) software were used for the random huminite reflectance measurements by taking 50 counts per each sample. ISO 7404–1 (2016) and ISO–11760 (2018) standards are used for coal rank determination. The analysis of macerals was done by taking 500 counts each with the help of an automatic point counter which works along with the Petroglite 4(x64) (version 2.35) software. The descriptions of macerals and terminologies as provided by the ICCP for huminite (Sýkorová et al., 2005), for liptinite (Pickel et al., 2017), and inertinite (ICCP, 2001) were followed. Leica application suite X (LAS) (5.0.3.24880 version) software was used for the photomicrography. The maceral photomicrographs were taken
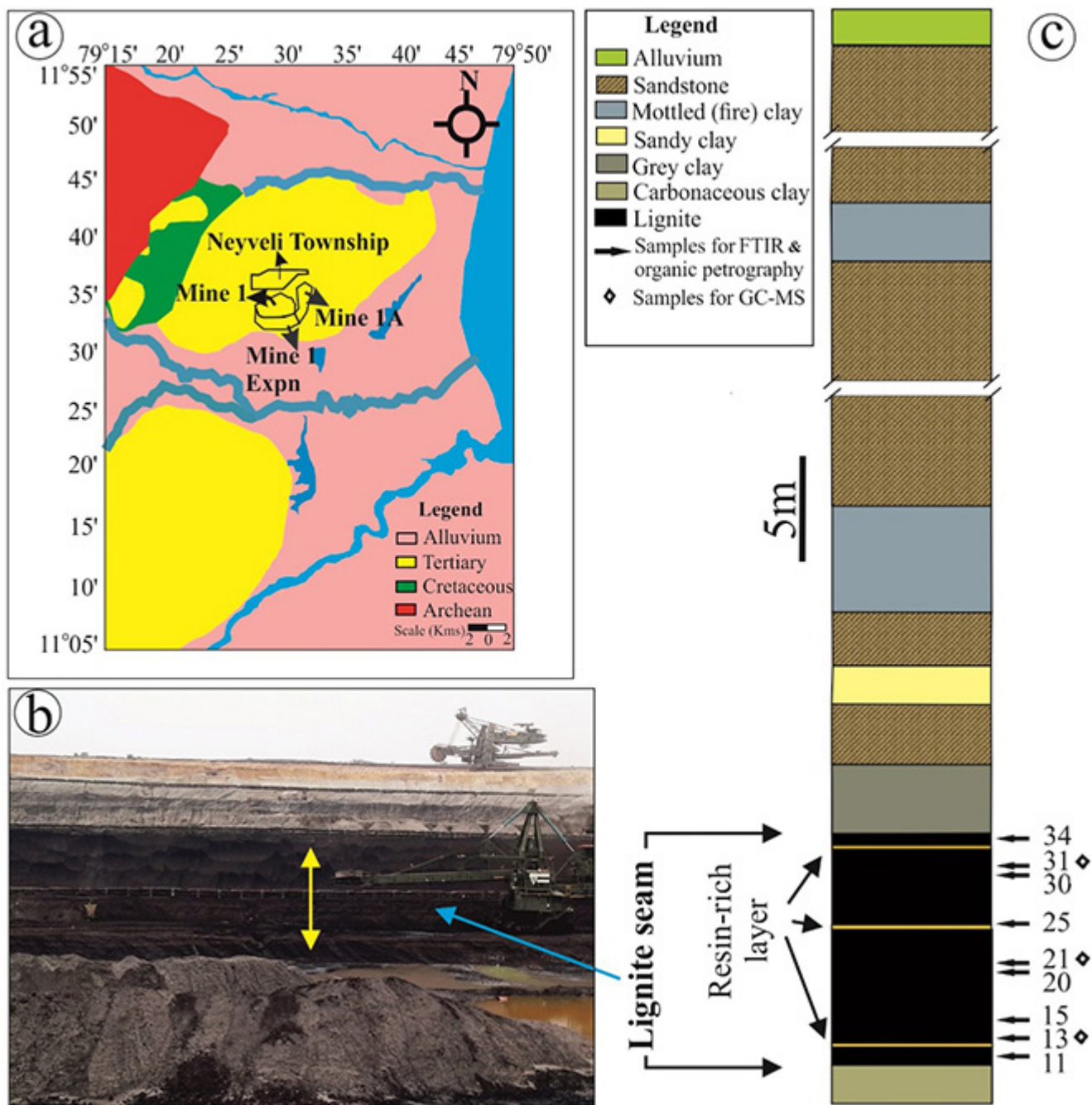
Fig. 2—(a) Geological plan of Neyveli Lignite Field with Mine–1 (after Anandan *et al.*, 2010); (b) field photograph of the Neyveli Lignite Mine–1; (c) litholog of Neyveli Lignite Mine–1 showing the lithological units and the position of the samples.

in normal incident/reflected light and the photomicrographs of fluorescing macerals are taken in blue light excitation mode.

Fourier Transform Infrared Spectroscopy

KBr pellet method which is a traditional FTIR sampling method commonly practiced for the analysis of solid dark

samples was used in this study. The samples were first ground into a fine powder and both the powder samples and KBr were kept in the hot air oven at 40°C for 12 h (He *et al.*, 2017) to reduce the influence of moisture on the FTIR spectrum. The sample and the KBr were mixed in a 1: 100 ratio and ground for 2 min. The mixture was transferred into the KBr die and pressed into pellets under 10 Mpa pressure for 1.30

min using a hydraulic pellet presser. Agilent Cary 630 FTIR Spectrometer with transmission sampling module was used for the spectral measurement and the control software was Microlab PC. The range of the spectral data was 4000–650 cm⁻¹ with a resolution of 4 cm⁻¹. The number of sample scans and background scans was 128 each. The area under the selected spectral peaks was calculated using Origin software.

Organic geochemistry using Gas Chromatography– Mass Spectrometry

For analysing *n*–alkane composition, three selected representative samples were powdered and then treated with dichloromethane and methanol in a ratio of 9: 1 and kept in an ultrasonicator for 30 min to obtain the bitumen. The bitumen obtained was then precipitated by adding an excess amount of *n*–hexane to remove the asphaltenes. Then the dried filtrate was separated into saturates and aromatics using column chromatography as given by Singh *et al.*, 2017. Only the saturated fraction was used for the GC–MS analysis for this study. Agilent 7890B Gas Chromatograph connected with Agilent 5977A Mass Spectrometer was used, which has an HP–5MS capillary column containing fused silica and the column has dimensions of 30 m × 0.25 mm inner diameter and 0.25 μm film thickness. Carrier gas was helium and the flow rate was set to 1ml/min. The oven temperature of the GC was initially 40°C which was maintained for 5 minutes and then it was ramped up to 310°C at a rate of 4°C per min. This top temperature was maintained for an additional 5.5 min. Mass spectra were obtained in the range of *m/z* 50–550 with an electron energy of 70 eV and a source temperature of 300 °C. Chemstation software was used for data processing. Peak assignments were made based on the retention time of the compounds in the GC and their mass spectral data. Only the *n*–alkane peaks were considered.

RESULTS

Organic petrography

The huminite, liptinite, and inertinite maceral groups and mineral matter were identified in all of the samples and their frequency distribution is listed in Table 1. The graphical representation of the relative percentage of the maceral groups in the samples is given in Fig. 3.

Huminite Group

The Neyveli Lignite Mine–1 has an approximate average of ~78 vol.% of the huminite group of macerals ranging from ~61 vol.% to ~93 vol.% and consisting of almost all the huminite group of macerals and submacerals except gelinite. The huminite group predominantly consists of detrohuminite
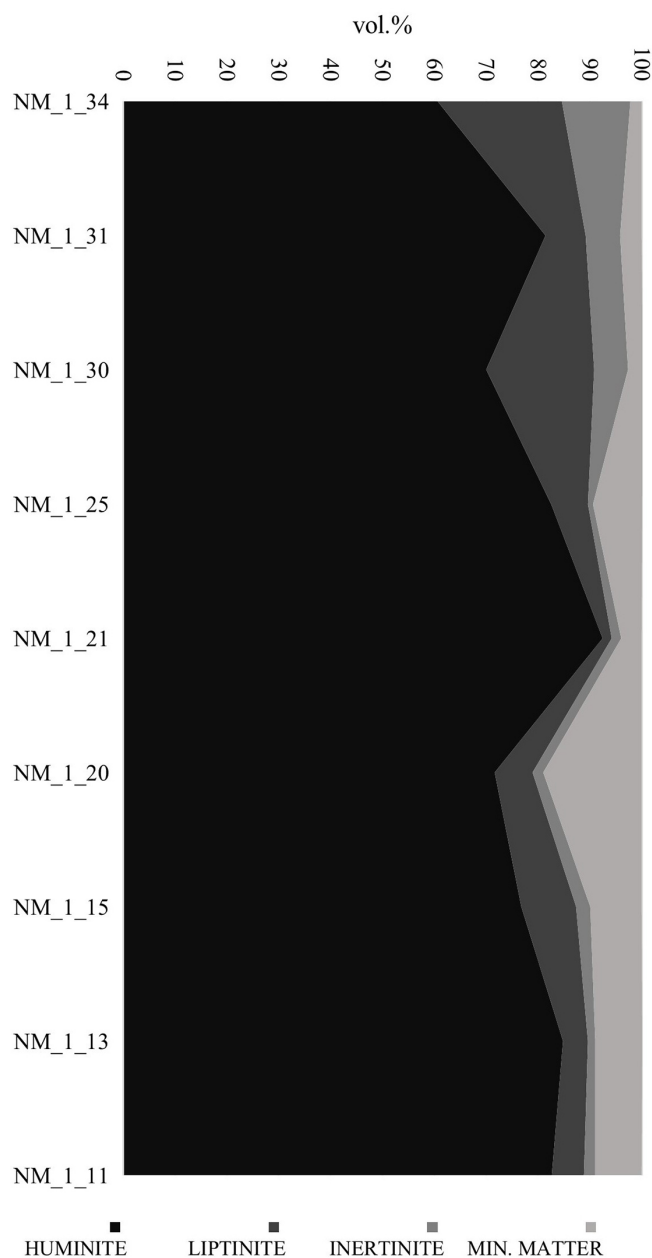
Fig. 3—The diagram representing variation in the maceral composition (vol. %) in the studied samples.

(attrinite + densinite) with an average vol.% of about 55 and ranging from ~42 vol.% to ~72 vol.%. The telohuminite [ulminite (Fig. 4a) + textinite (Fig. 4b)] consists of an average vol.% of about 21 and ranges from ~11 vol.% to ~31 vol.%. Gelohuminite–the gelified macerals of huminite is mainly represented by corpohuminite (Fig. 4c) which consists of an approximate average of 3 vol.% and ranges from ~0 vol.% to ~5 vol.%. Among the detrohuminite, densinite (Fig. 4d) is the main constituent ranging from ~34 vol.% to ~72 vol.%.

Table 1—Macerals and mineral matter content (vol.%), huminite reflectance (R_r %) and the calculated petrographic indices (GI, TPI, GWI, VI) of the studied samples.

Sample No.		NM_1_11	NM_1_13	NM_1_15	NM_1_20	NM_1_21	NM_1_25	NM_1_30	NM_1_31	NM_1_34	Average	Minimum	Maximum	Standard deviation
Macerals														
Huminite(H)		82.68	84.84	76.80	71.58	92.45	82.58	70.00	81.44	60.66	78.11	60.66	92.45	9.47
Telohuminite		31.29	10.90	20.44	16.32	30.67	16.58	25.50	22.68	14.21	20.95	10.90	31.29	7.18
	Textinite	6.70	2.37	3.87	0.00	3.11	0.00	0.00	2.58	0.00	2.07	0.00	6.70	2.33
	Ulminite	24.58	8.53	16.58	16.32	27.56	16.58	25.50	20.10	14.21	18.88	8.53	27.56	6.12
Detrohuminite		51.40	72.04	54.14	52.63	60.45	62.00	42.00	53.61	43.72	54.66	42.00	72.04	9.26
	Attrinite	0.56	0.47	2.21	13.68	1.78	5.00	8.00	1.03	2.19	3.88	0.47	13.68	4.40
	Densinite	50.84	71.56	51.93	38.95	58.67	57.00	34.00	52.58	41.53	50.78	34.00	71.56	11.43
Gelohuminite		0.00	1.90	2.21	2.63	1.33	4.00	2.50	5.16	2.73	2.50	0.00	5.16	1.48
	Corpohuminite	0.00	1.90	2.21	2.63	1.33	4.00	2.50	5.16	2.73	2.50	0.00	5.16	1.48
	Gelinite	0.00	0.00	0.00	0.00	0.00	0.00	0.00	0.00	0.00	0.00	0.00	0.00	0.00
Liptinite (L)		6.15	4.79	10.50	7.37	1.78	7.00	20.84	7.73	24.00	10.02	1.78	24.00	7.45
	Sporinite	0.00	0.00	2.76	1.58	0.00	1.00	1.50	1.55	4.37	1.42	0.00	4.37	1.45
	Cutinite	2.24	0.00	2.76	0.53	0.00	1.00	1.00	0.52	1.09	1.01	0.00	2.76	0.94
	Suberinite	0.00	0.00	0.00	2.63	0.00	0.00	0.50	3.61	0.00	0.75	0.00	3.61	1.38
	Resinite	2.79	2.84	0.55	1.58	1.78	1.00	2.50	0.00	6.56	2.18	0.00	6.56	1.92
	Alginite	0.56	1.47	0.00	0.00	0.00	0.00	0.00	0.00	0.00	0.23	0.00	1.47	0.50
	Bituminite	0.00	0.00	0.00	0.00	0.00	0.00	0.50	0.00	0.50	0.11	0.00	0.50	0.22
	Fluorinite	0.00	0.00	0.00	0.00	0.00	0.00	0.00	0.00	0.00	0.00	0.00	0.00	0.00
	Exsudatinite	0.00	0.00	0.00	0.00	0.00	0.00	0.34	0.52	0.00	0.09	0.00	0.52	0.19
	Liptodetrinite	0.56	0.47	4.42	1.05	0.00	4.00	14.50	1.55	11.48	4.23	0.00	14.50	5.25
Inertinite (I)		2.24	1.42	2.76	2.11	1.78	1.00	6.50	6.70	13.12	4.18	1.00	13.12	3.96
	Semifusinite	0.00	0.00	0.00	1.05	0.00	0.00	1.00	0.00	7.10	1.02	0.00	7.10	2.33

Fusinite	0.00	0.00	0.00	0.00	0.00	0.00	0.00	0.00	0.00	0.00	0.00	0.00	0.00
Funginite	2.24	1.42	2.76	1.05	1.78	1.00	5.50	6.70	6.01	3.16	1.00	6.70	2.27
Secretinite	0.00	0.00	0.00	0.00	0.00	0.00	0.00	0.00	0.00	0.00	0.00	0.00	0.00
Macrinite	0.00	0.00	0.00	0.00	0.00	0.00	0.00	0.00	0.00	0.00	0.00	0.00	0.00
Micrinite	0.00	0.00	0.00	0.00	0.00	0.00	0.00	0.00	0.00	0.00	0.00	0.00	0.00
Inertodetrinite	0.00	0.00	0.00	0.00	0.00	0.00	0.00	0.00	0.00	0.00	0.00	0.00	0.00
Mineral Matter (M) (TOTAL)	8.92	9.01	9.94	18.95	4.00	9.50	2.80	4.12	2.19	7.71	2.19	18.95	5.23
Others	8.92	9.01	9.94	18.95	4.00	9.50	2.80	4.12	2.19	7.71	2.19	18.95	5.23
Pyrite	0.00	0.00	0.00	0.00	0.00	0.00	0.00	0.00	0.00	0.00	0.00	0.00	0.00
Fluorescing H	54.75	73.46	47.51	53.68	68.54	59.92	41.00	53.61	42.62	55.01	41.00	73.46	10.94
Non-fluorescing (H)	27.93	11.37	29.28	17.89	23.90	22.66	29.00	27.83	18.03	23.15	11.37	29.28	6.22
Total Fluorescing (H+L)	60.89	78.25	58.01	61.05	70.32	66.92	61.84	61.34	66.62	65.33	58.01	78.25	6.27
Non-fluorescing (H+I+M)	39.09	21.80	41.98	38.95	29.68	33.16	38.30	38.66	33.33	34.71	21.80	41.98	6.27
H (mmf)	90.80	93.18	85.28	88.31	96.30	91.17	71.91	84.95	62.04	88.13	62.04	96.30	11.04
L (mmf)	6.75	5.26	11.66	9.09	1.85	7.73	21.41	8.06	24.54	9.11	1.85	24.54	7.49
I (mmf)	2.45	1.56	3.07	2.60	1.85	1.10	6.68	6.99	13.41	2.76	1.10	13.41	3.99
R_r mean %	0.33	0.37	0.37	0.34	0.35	0.40	0.43	0.40	0.43	0.37	0.33	0.43	0.04
GI	7.94	19.22	8.00	3.67	13.13	12.93	4.28	7.55	3.82	9.88	3.67	19.22	5.23
TPI	0.61	0.18	0.42	0.38	0.53	0.33	0.69	0.52	0.55	0.45	0.18	0.69	0.16
GWI	1.88	7.25	2.83	2.02	1.97	3.27	1.17	2.61	2.83	2.91	1.17	7.25	1.76
VI	0.62	0.19	0.33	0.39	0.54	0.26	0.50	0.46	0.46	0.40	0.19	0.62	0.14

GI (Gelification Index) = (Ulminite+Densinite+Corpohuminite+Gelinite)/(Textinite+Attrinite+Inertinite) (Kalaitzidis et al., 2004).

TPI (Tissue Preservation Index) = (Textinite+Ulminite+Corpohuminite+Fusinite+Semifusinite)/(Attrinite+Densinite+Gelinite+Inertodetrinite) (Kalaitzidis et al., 2004).

GWI (Ground Water Index) = (Densinite+Corpohuminite+Gelinite+Mineral matter)/(Textinite+Ulminite+Attrinite) (Kalaitzidis et al., 2004).

VI (Vegetation Index) = (Textinite+Ulminite+Suberinite+Resinite+Fusinite+Semifusinite)/(Attrinite+Densinite+Cutinite+Sporinite+Alginite+Bituminite+Liptodetrinite+Inertodetrinite) (Kalaitzidis et al., 2004)
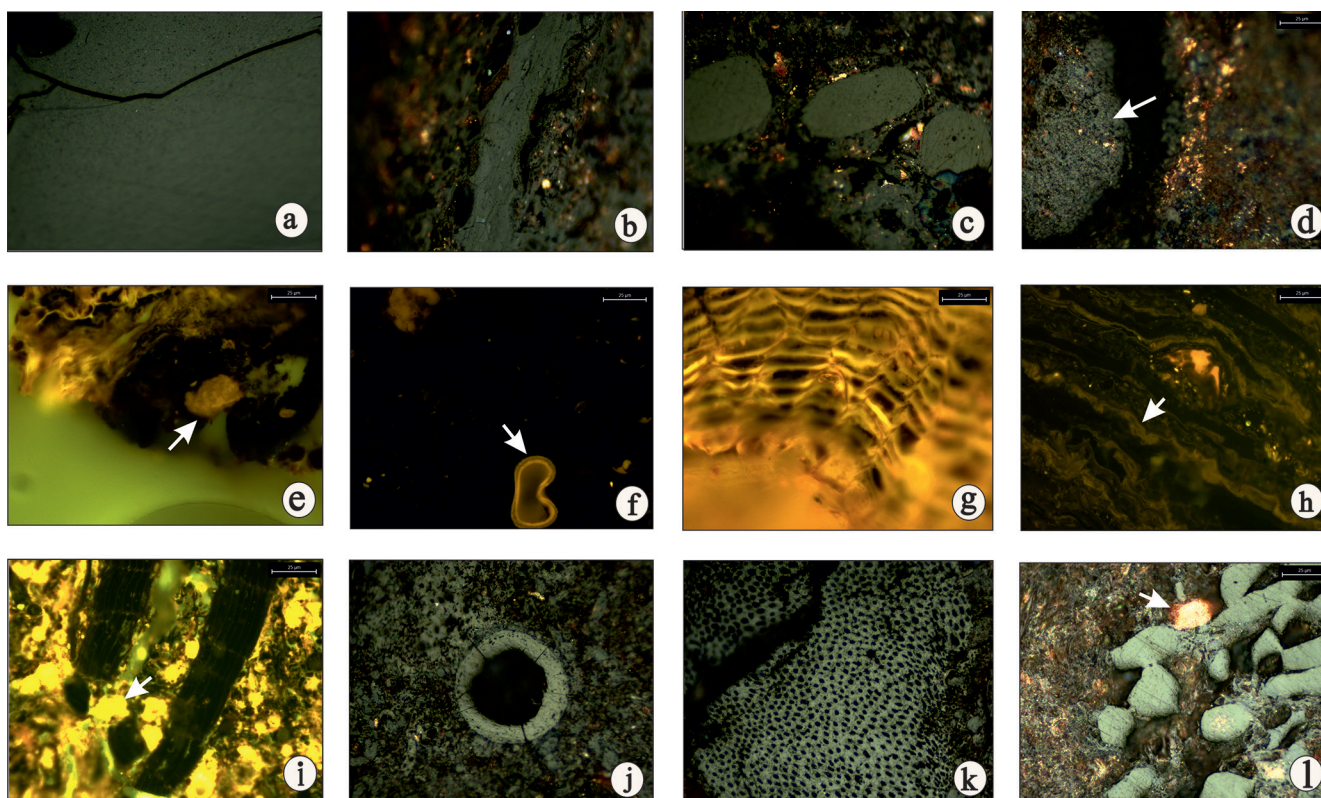
Fig. 4—Representative photomicrographs of macerals and mineral matter. a) ulminite; b) textinite; c) corpohuminite; d) densinite; e) telalginite; f) sporinite; g) suberinite; h) cutinite; i) resinite; j) funginite; k) semifusinite; l) mineral matter. Photomicrographs were taken under reflected white light (a–d, j–l) and in fluorescence mode (e–i).

Liptinite Group

The total liptinite content in the Neyveli Lignite Mine–1 is an approximate average vol.% of 10 and ranges from ~2 vol.% to ~24 vol.%. Alginite (Fig. 4e) is found in very minor amount (avg. vol.% about 0.23) while liptodetrinite (~0.00 to ~15.00 vol.%), sporinite (Fig. 4f) (~0 to ~4 vol.%), suberinite (Fig. 4g) (~0 to ~4 vol.%), cutinite (Fig. 4h) (~0 to ~3 vol.%) and resinite (Fig. 4i) (~0 to ~7 vol.%) were common in almost all the studied samples. Solid bitumen was also identified in these samples although very less.

Inertinite Group

The inertinite group of macerals present in the Neyveli Lignite Mine–1 has an approximate average vol.% of 4 ranging from ~1 to ~13 vol.%. Funginite (Fig. 4j) is the most found inertinite maceral which has an average vol.% of about 3 and ranges from ~1 to ~7 vol.%. The next found maceral in this group is semifusinite (Fig. 4k) with an average vol.% of about 1% and ranges from ~0 to ~7 vol.%. Other inertinite macerals were absent. The Neyveli Lignite Mine–1 contains an appreciable amount of mineral matter (Fig. 4l) of an average of about 8.00 vol.% ranging from ~2.00 to ~19.00 vol.%. Pyrite is absent.

Organic petrographic facies indices

The calculated petrographic facies indices are provided in Table 1. Gelification Index (GI) values range from 3.67 to 19.22 (avg. 9.88), Tissue preservation Index (TPI) values range from 0.18 to 0.69 (Avg. 0.45), Ground Water Index (GWI) values range from 1.17 to 7.25 (avg. 2.91) and values of Vegetation Index (VI) are ranging from 0.19 to 0.62 (Avg. 0.40). The reflectance values are listed in Table 1. The huminite (ulminite) reflectance of the Neyveli Lignite Mine–1 is ranging from ~0.33 to ~0.43 R_r% and has an average value of 0.37 R_r%.

FTIR Spectroscopy

The representative FTIR spectra of Neyveli Lignite Mine–1 are shown in the Fig. 5. The broad band ranging from 3656–3226 cm^{-1} generally indicates Hydroxyl (OH) groups. However, it should also be noted that pyrrolic–NH and kaolinite hydroxyls are also found in these region (Sen *et al.*,
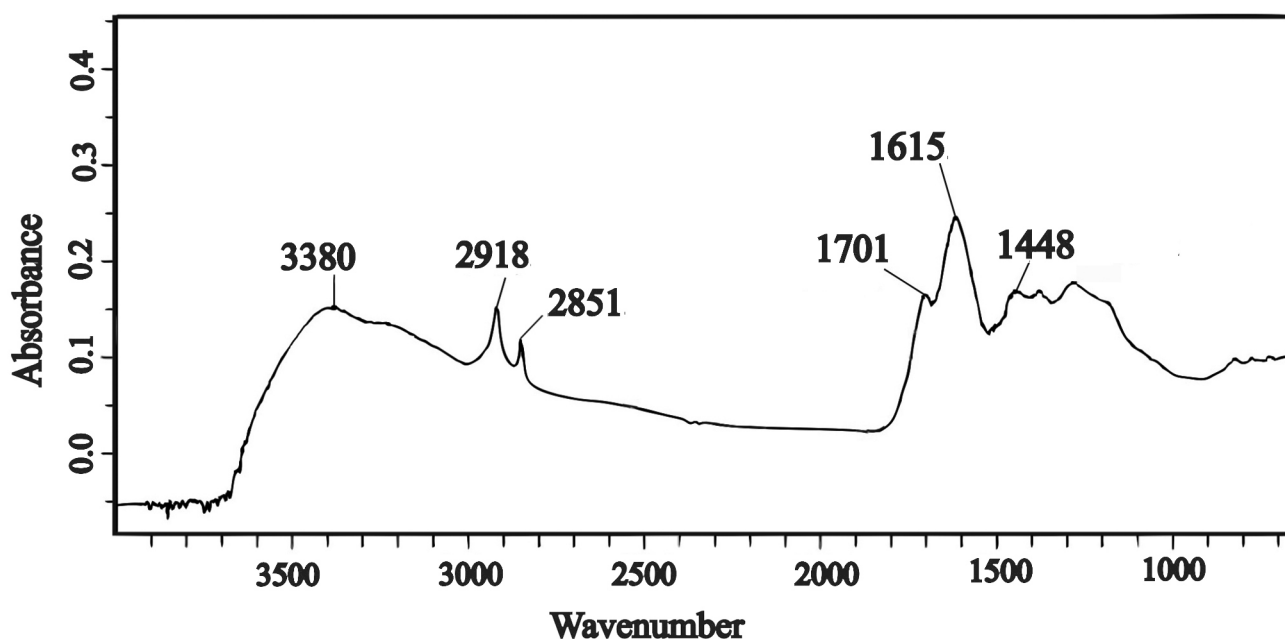
Fig. 5—Representative FTIR spectra of the studied sample showing major peak assignments.

2022). C–H aliphatic stretching regions are identified between 2847–2954 cm^{-1}. The peaks found at a region ranging from 1377–1451 cm^{-1} are characterised as aliphatic C–H bending peaks. The aromatic C=O is identified at 1650 cm^{-1} and C=C stretching is identified ranging from 1550 cm^{-1}–1615 cm^{-1}. The 'A'–Factor and 'C'–Factor are calculated using the band area and are given in Table 2. The relative intensity changes of the aliphatic groups are represented by 'A'–Factor, and the variations in C=O groups are represented by 'C'–Factor (Ganz & Kalkreuth, 1987; Guo & Bustin, 1998). The kerogen type as well as the maturation levels of the samples can be inferred from the A factor and C factor.

GC–MS

The *n*–alkanes range from n–C_{14} to n–C_{35} and are observed in the samples with unimodal and bimodal distributions (Fig. 6). However, although both distributions are evident, the maximum relative abundance that is, carbon number maximum (C_{max}) is shown by n–C_{27} for all the samples. C_{max} can be generally used to understand the source of organic matter source (Mallick *et al.*, 2021). Moreover, the *n*–alkanes distribution shows a predominance of long–chain (>n–C_{25}) over mid–chain (n–C_{21} to n–C_{25}) *n*–alkanes, while short–chain *n*–alkanes (less than n–C_{21}) occur in low quantities.

Table 2—The area under the region and the calculated A–factor and C–factor for the studied samples.

Sample ID	3000-2800 cm^{-1}	1650-1520 cm^{-1}	1800-1650 cm^{-1}	C-Factor	A-Factor
NM_1_11	4.19	10.73	2.44	0.19	0.28
NM_1_13	16.16	11.11	2.18	0.16	0.59
NM_1_15	4.22	7.55	1.17	0.13	0.36
NM_1_20	2.64	8.69	1.43	0.14	0.23
NM_1_21	2.96	10.57	2.88	0.21	0.22
NM_1_25	8.54	8.36	2.42	0.22	0.51
NM_1_30	5.78	11.64	2.10	0.15	0.33
NM_1_31	1.60	3.91	0.78	0.17	0.29
NM_1_34	8.37	11.37	2.57	0.18	0.42

$A-Factor = (2800 - 3000\ cm^{-1})/(2800 - 3000\ cm^{-1}) + (1650 - 1520\ cm^{-1})$
$C-Factor = (1650 - 1800\ cm^{-1})/(1650 - 1800\ cm^{-1}) + (1650 - 1520\ cm^{-1})$
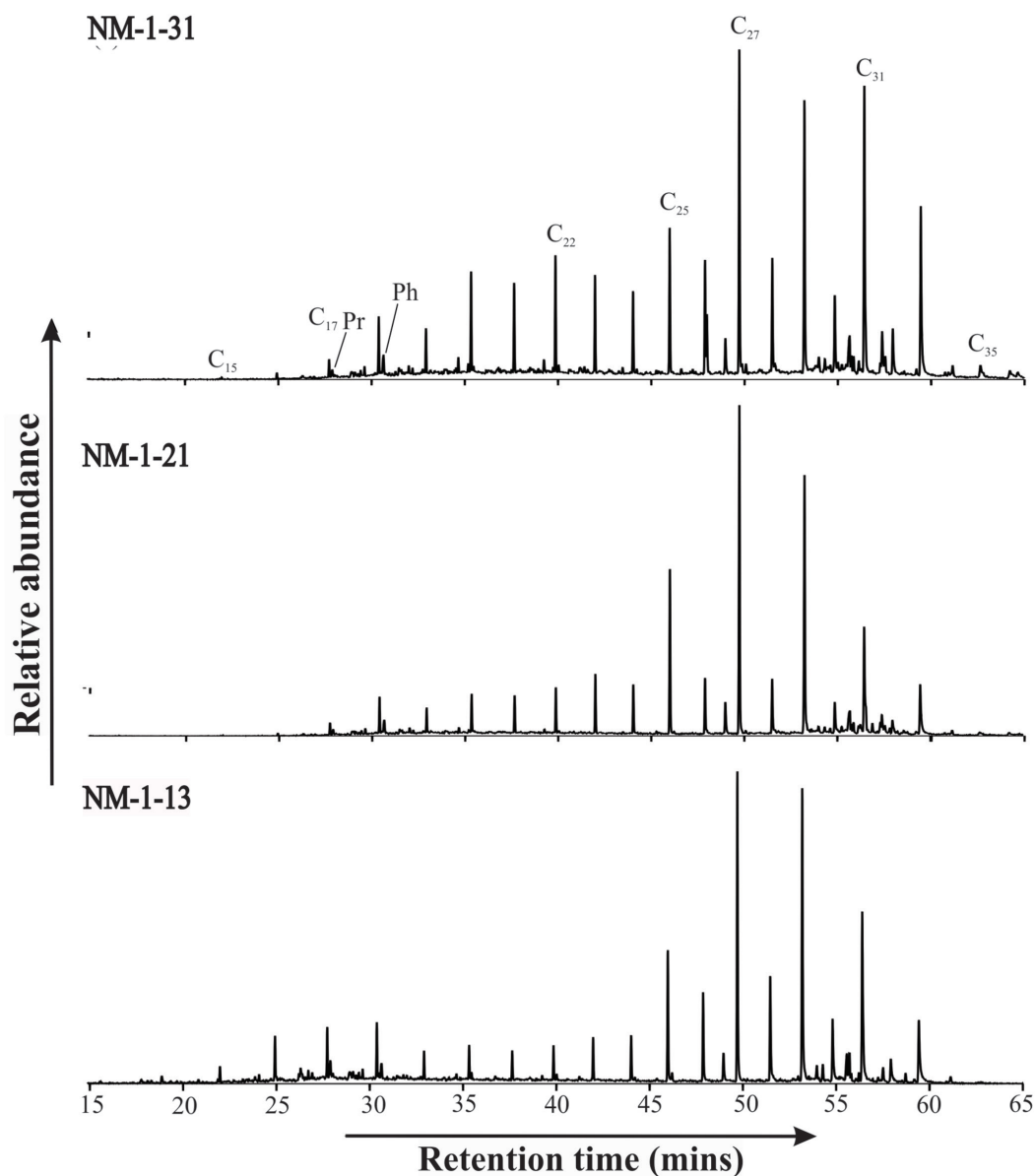
Fig. 6—Partial chromatogram (*m/z* 57) showing *n*–alkane distribution in the studied samples (Numbers corresponds to the number of carbons in the *n*–alkane chain).

Different parameters of alkanes have been estimated and are provided in Table 3. The carbon preference index (CPI: Peters *et al.*, 2005) ranges between ~2.09 and ~4.20 with an average of about 3.16. The terrigenous/ aquatic ratio (TAR: Bourbonniere & Meyers, 1996) varies from ~10.04 to ~24.23 with an average of about 17.27. The pristane/phytane (Pr/Ph) ratio is varying from ~0.43 to ~1.16 in the studied samples. The proxy wax (P_{wax}: Zheng *et al.*, 2007) varies from ~0.79 to ~0.84 with an average of about 0.81, and the proxy aqueous (P_{aq}: Ficken *et al.*, 2000) varies from ~0.23 to ~0.32. The aliphatic chain length (ACL) values (Eglinton & Hamilton, 1967) vary from ~28.33 to ~29.31 with an average of 28.81. The Pr/n–C_{17} ratio varies between 0.53 and 0.66 with an average of 0.62. Ph/n–C_{18} has a minimum value of 0.42 and a maximum value of 0.52 with an average of 0.49. $\Sigma\ C_{22}$–$/\Sigma\ C_{23}$+ ratio varies from 0.13 to 0.20 with an average value of 0.17. OEP values (Scalan & Smith, 1970) range from 1 to 2.87 with an average value of 1.78.

DISCUSSION

Palaeoflora

The lignite samples that were examined consist primarily of huminite, with the maceral groups such as liptinites and inertinites following closely behind. This composition suggests that there was a continuous influx of terrestrial matter, such as trees, herbs, shrubs, and bushes, which were deposited and preserved in a site with a high–water level (Singh *et al.*, 2021). Bimodal distribution indicates major organic matter input from dual sources. The bottom sample showing bimodal distribution indicates the mixed source of organic matter. High abundance of compounds with odd carbon numbers greater than 25 and maximising at n–C$_{27}$ in all the analysed samples. This indicates the terrestrial source higher plant input to the organic matter (Singh *et al.*, 2022). Less relative abundance of n–C$_{17}$ compared to longer alkanes and high relative abundance of short–chain alkanes compared to medium–chain alkanes in the NM–1–13 sample can be inferred that organic matter also contains algal or microbial input (Mathews *et al.*, 2020) and it is also supported by the presence of telalginite (Fig. 4e). The considerable amount of n–C$_{25}$ mid–chain alkane found in the samples indicates that there was also input from aquatic macrophytes (Ficken *et al.*, 2000). Additionally, the dominance of detrohuminite,

as indicated by the relatively higher presence of densinite (Fig. 4d) maceral suggests a significant contribution from herbaceous and bushy plants that easily decompose resulting in the formation of peat in subaqueous conditions, and the presence of perhydrous huminite suggests impregnation of liptinite maceral derived from higher plants (Singh *et al.*, 2021). The P$_{aq}$ value for the studied samples is ranging from 0.23 to 0.32 which depicts that the organic matter constitues emergent flora such as mangrove as source (Ficken *et al.*, 2000). The studied samples also contain a significant percentage of ulminite (Fig. 4a) along with the noticeable presence of liptinite macerals which suggests the existence of forested vegetation such as mangroves in the surrounding area (Singh *et al.*, 2017, 2021). A considerable amount of funginite (Fig. 4j) indicates microbial degradation of organic matter and supports the occurrence of a high amount of detrohuminite. The CPI values obtained range from 2.09 to 4.20 and the TAR values are also very high. This is typical for immature organic matter with a higher input of waxy plants (Peters *et al.*, 2005; Zivotic *et al.*, 2010). The P$_{wax}$ ratio obtained for the samples has values that indicate the input of wax from terrestrial as well as emergent plants (Zheng *et al.*, 2007). The Σ C$_{22}$–/Σ C$_{23}$+ ratio shows only very low values therefore we can infer that only a very small amount of terrestrial biomass was affected by bacterial degradation.

Table 3—The n–alkane indices/ratios calculated for the studied lignite samples.

SAMPLE ID	P$_{aq}$	P$_{wax}$	CPI	TAR	ACL	Pr/Ph	Pr/n-C$_{17}$	Ph/n-C$_{18}$	ΣC$_{22}$-/ΣC$_{23}$+	OEP
NM-1-13	0.23	0.84	3.18	10.04	28.78	1.16	0.53	0.42	0.19	2.87
NM-1-21	0.32	0.79	4.2	24.23	28.33	0.45	0.66	0.51	0.13	1.46
NM-1-31	0.26	0.81	2.09	17.56	29.31	0.43	0.66	0.52	0.20	1.00
Maximum	0.32	0.84	4.2	24.23	29.31	1.16	0.66	0.52	0.2	2.87
Minimum	0.23	0.79	2.09	10.04	28.33	0.43	0.53	0.42	0.13	1.00
Standard Deviation	0.05	0.03	1.06	7.10	0.49	0.42	0.08	0.06	0.04	0.97
Average	0.27	0.81	3.16	17.27	28.81	0.68	0.62	0.49	0.17	1.78

Pr: Pristane, Ph: Phytane, P$_{aq}$: Proxy aqueous, P$_{wax}$: Proxy wax, CPI: Carbon Preference Index, TAR: Terrigenous/Aquatic Ratio, ACL: Aliphatic chain length, OEP: Odd Even Predominance.

P$_{aq}$ = (C$_{23}$ + C$_{25}$) / (C$_{23}$+ C$_{25}$+ C$_{29}$+ C$_{31}$) Ficken *et al.*, 2000.

P$_{wax}$ = (C$_{27}$+ C$_{29}$+ C$_{31}$) / (C$_{23}$ + C$_{25}$ + C$_{27}$ + C$_{29}$ + C$_{31}$) Zheng *et al.*, 2007.

CPI = 2(C$_{23}$ + C$_{25}$ + C$_{27}$ + C$_{29}$) / [C$_{22}$ + 2(C$_{24}$ + C$_{26}$ + C$_{28}$) + C$_{30}$] Peters *et al.*, 2005.

TAR = (C$_{27}$ + C$_{29}$ + C$_{31}$) / (C$_{15}$+ C$_{17}$ + C$_{19}$) Bourbonniere & Meyers (1996).

ACL = (25C$_{25}$ + 27C$_{27}$ + 29C$_{29}$ + 31C$_{31}$ + 33C$_{33}$) / (C$_{25}$ + C$_{27}$ + C$_{29}$ + C$_{31}$ + C$_{33}$) Eglinton & Hamilton (1967).

OEP = (C$_{21}$+6C$_{23}$+C$_{25}$) / (4C$_{22}$+4C$_{24}$) Scalan & Smith (1970).

Palaeodepositional settings

To comprehend the patterns of deposition, a combination of maceral compositions, organic facies indices and *n*–alkane geochemical parameters are used. The TPI index is utilised to assess the extent of humification in the organic matter that forms peat, while the GI index measures the moisture content in the peat–forming environment in relation to the destruction of plant cells. A high TPI value indicates a balance between the growth and accumulation of plant materials, an increase in the water table, and the prevalence of tree vegetation. A low TPI value suggests either the dominance of herbaceous plants in the peatland or significant degradation of plant tissues due to advanced humification. On the other hand, a high GI value signifies a high–water level and substantial gelification in the peat–forming environment (Singh *et al.*, 2017). The studied lignite samples have a high GI (3.67–19.22, avg. 9.88) and low to moderate TPI values (0.18–0.69, avg. 0.45). This indicates that the deposition of the precursors of peat took place in a limno–telmatic regime. The noteworthy fluctuations observed in these measurements signify notable alterations in the input of vegetation sources and bacterial degradation processes (Mathews *et al.*, 2020). Also, the GI–TPI facies model (Fig. 7a) (after Diessel, 1992) depicts that the samples are formed in a limno–telmatic regime.

The coal facies model (Fig. 7b) introduced by Calder *et al.* (1991) based on the GWI (groundwater index) and VI (vegetation index) indices was later adapted by Kalaitzidis *et al.* (2000) specifically for low–rank Cenozoic lignite. The GWI index serves as an indicator of the groundwater level and relative rainfall during the accumulation of peat. When the GWI value is less than 0.5, it suggests ombrotrophic hydrological conditions, whereas values exceeding 1 indicate rheotrophic hydrological conditions. A mesotrophic hydrological condition is characterised by GWI values ranging between 0.5 and 1. On the other hand, the VI index is associated with the vegetation type found in the mire (Singh *et al.*, 2017). The GWI values obtained for the studied samples have a value ranging from 1.17 to 7.25 which suggests that they are formed at mesotropic to rheotropic hydrological conditions. The low VI values contribute to the result that the samples will come under limno–telmatic condition.

The ternary diagram (Fig. 7c) proposed by Mukhopadhyay, 1986 showing the facies–critical maceral assemblages in the lignite and the proposed environment of peat formation depicts that the organic matter was deposited in a suboxic condition with bacterial degradation of the OM. It is supported by the very low abundance of inertinites, which indicates that there were only minimal forest/peat fires or oxidation and had a waterlogged condition probably due to the result of periodic flooding (Singh *et al.*, 2017). The occurrence of flooding events is further supported by the ternary ABC–facies model (Fig. 7d) based on the maceral composition (Singh *et al.*, 2010a). The model suggests that the samples were deposited in a wet moor setting with significant flooding events and there was intermediate tissue preservation. The presence of macerals like corpohuminite and textinite validates this point. The Pr/Ph ratio of the studied samples has a value ranging from 0.43 to 1.16 which indicates that the bottom part is formed during a moderate environment and as we go to the top parts of the seam, the values show it is formed under more reducing conditions (Mathews *et al.*, 2020). The Pr/*n*–C$_{17}$ vs. Ph/*n*–C$_{18}$ plots (Fig. 8a, b) and Fig. 8c indicates that they are formed in a transitional environment most probably in a lagoonal condition with moderate redox conditions.

The considerable concentrations of funginite in the samples suggest warm and humid/moist climatic conditions. However, these conditions do not lead to the oxidation of peat and biomass combustion (Ghosh *et al.*, 2022), as indicated by the low concentrations of other macerals in the inertinite group produced by oxidation. These conditions are favourable for the growth of fungi and lush vegetation in tropical to sub–tropical climates (Singh *et al.*, 2017). This interpretation is also supported by ACL values. The ACL serves as a valuable tool for reconstructing past palaeoclimatic conditions that supported the growth of peat–forming vegetation (Singh *et al.*, 2021). The basic concept underlying the use of this proxy is that vascular land plants in warmer climates produce longer chain wax lipids compared to those in cooler climates, as a mechanism to prevent water loss during transpiration (Andersson *et al.*, 2011). Hence, warmer the temperature, higher will be the ratio. In the studied samples, the ACL values range from 28.33 to 29.31 which suggest that the deposition period was with a moderately warmer and humid climate (Karadirek, 2023). A variation diagram of P$_{aq}$, P$_{wax}$ and ACL values (Fig. 9) has been prepared following Kumar *et al.* (2021). It has been observed that as ACL increases, the P$_{wax}$ is increasing and P$_{aq}$ is decreasing correspondingly which indicate the relationship of climate with floral input and hydrological conditions which is consistent with the observations of Kumar *et al.* (2021).

Type of kerogen and hydrocarbon Potential

Earlier works on organic matter related to hydrocarbon exploration shows four primary classifications of kerogen (Killops & Killops, 1993; Hunt, 1994). Sapropelic kerogen, known as type–I, is derived from algaenan and exhibits a significant potential for the production of oil. Liptinic kerogen, or type–II, is capable of generating both oil and gas. type–III, also known as humic kerogen, is predominantly associated with gas production and is formed as peat on the earth's surface. Type–IV kerogen consists of extensively altered organic matter which is of higher plant origin (Matthewman *et al.*, 2013). The pseudo–Van–Krevelen plot (Fig. 10) of calculated A–factor versus C–factor derived from the FTIR spectra of the studied samples shows that the samples are plotted in–between type–II and type–III range signifying
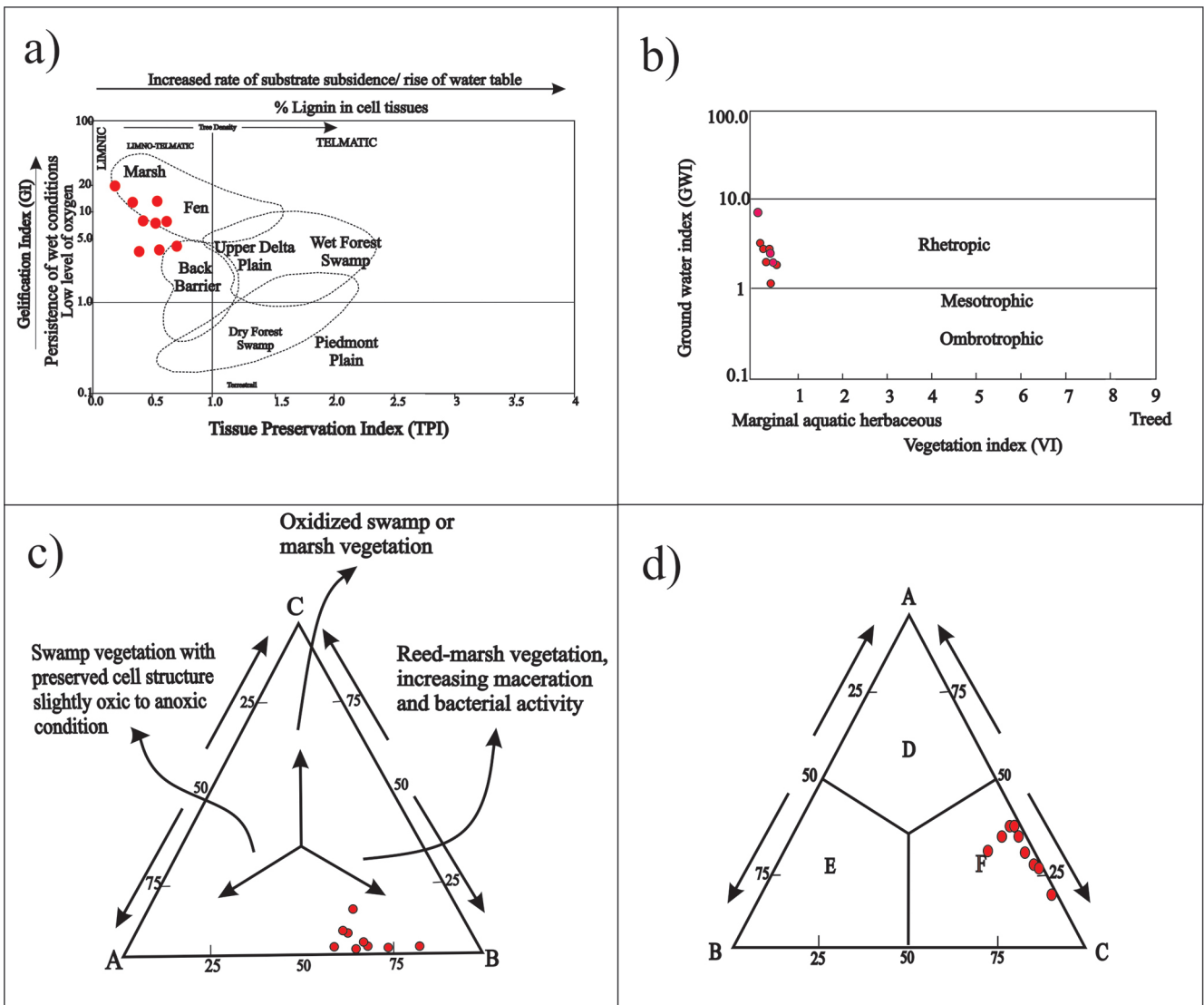
Fig. 7—(a) Facies interpreted from the GI v/s TPI indices in relation to depositional settings and mire type; (b) Diagram of GWI v/s VI showing relationship between vegetation type and hydrological conditions; (c) Ternary diagram showing facies–critical maceral associations in lignite and suggested peat forming palaeoenvironment were, A= telohuminite + corpohuminite + sporinite + cutinite + resinite + suberinite, B= detrohuminite + gelinite + liptodetrinite + alginite, C= inertinite; (d) Ternary diagram showing the peat forming environment of the studied samples were, A= telohuminite + gelohuminite + sporinite + cutinite + resinite + suberinite, B= fusinite + semifusinite + macrinite (as ground mass) + secretinite + funginite, C= clastic mineral matter + detrohuminite + inertodetrinite + liptodetrinite + discrete macrinite + alginite, D=wet moor having moderate flooding with moderate to good tissue preservation, E=oxic (dry) moor with increased tissue preservation, F=wet moor with high flooding and low to moderate tissue preservation.

mixed type II/III kerogen with potential for generating mostly gas with some oil. The ternary diagrams, following Hakimi *et al.*, 2023 which is plotted on the basis of the percentage of macerals and are used to infer the type of kerogen (Fig. 11a) and hydrocarbon source potential (Fig. 11b) of the samples. The diagrams indicate that the samples are coming under type–III kerogen. However, two samples show that they are oil and gas–prone. The presence of solid bitumen is an indicator that the kerogen has attained a level of maturity required to yield hydrocarbons and the solid bitumen found here is pre–oil bitumen which can serve as an indicator for the slight transformations that are occurring in the parent kerogen (Mastalerz *et al.*, 2018). Solid bitumen serves as an indicator
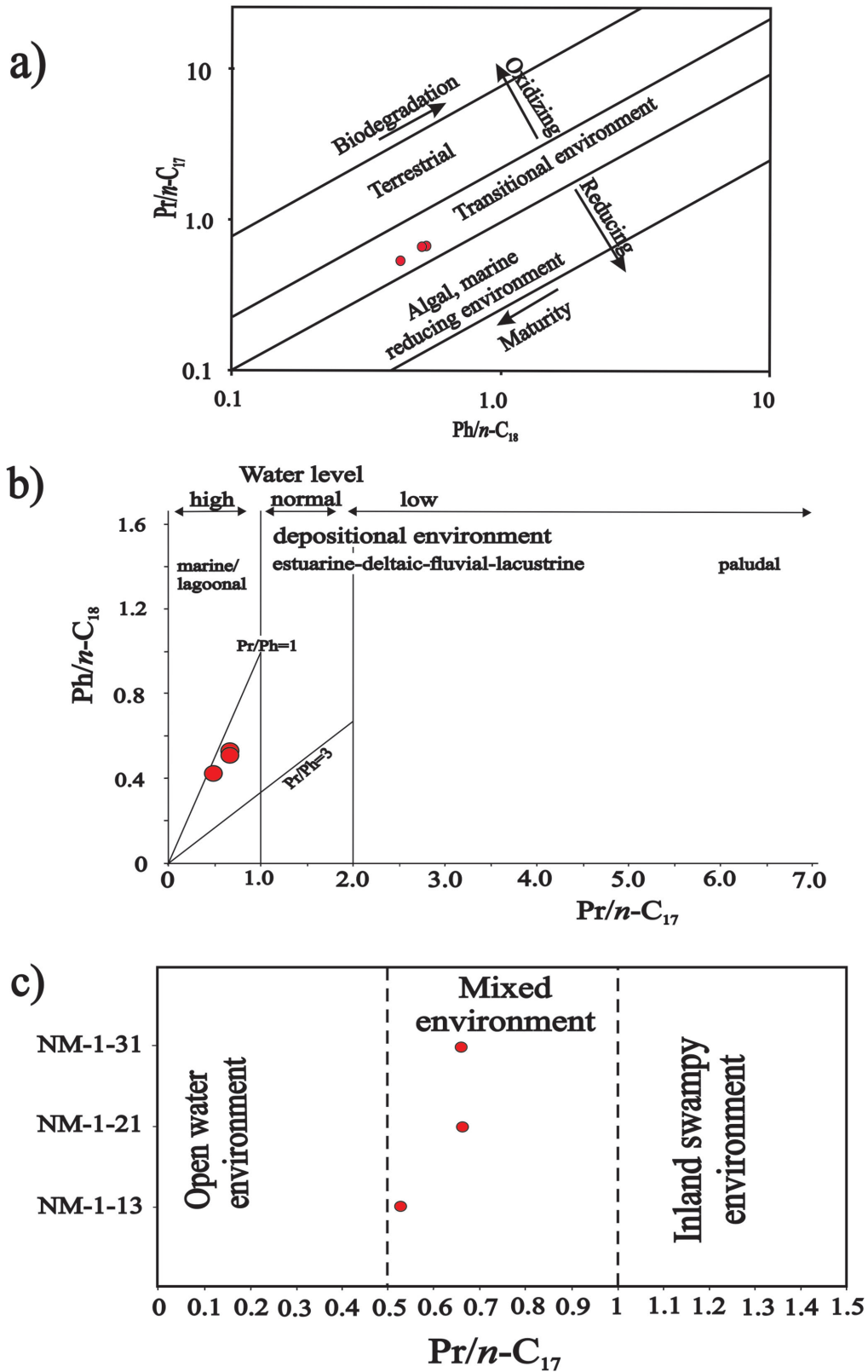
Fig. 8—(a) Pristane/n–C_{17} vs. phytane/n–C_{18} plot exhibiting the organic matter input and redox conditions during deposition of the studied samples; (b) The Pr/n–C_{17} vs. Ph/n–C_{18} diagram (after Gola *et al.*, 2013); (c) Pr/n–C_{17} values indicating organic matter depositional environment of the samples (after Kumar *et al.*, 2021).
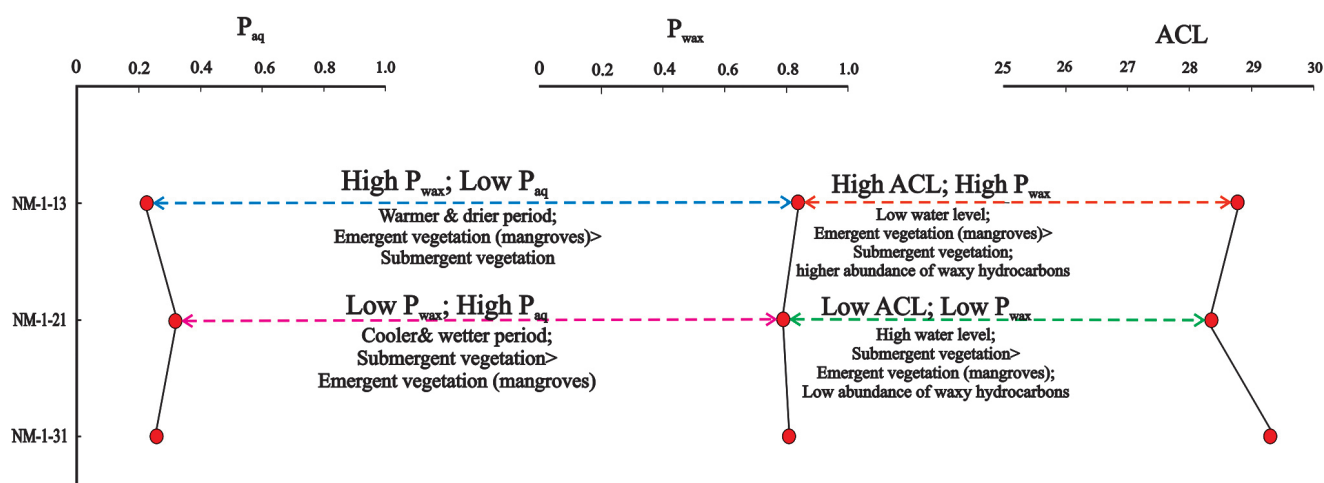
Fig. 9—Showing the correlation between P_{wax}, P_{aq} and ACL.

of oil and gas reservoirs due to its status as a byproduct of petroleum and natural gas (Li *et al.*, 2020).

Thermal maturity of kerogen

The Huminite reflectance value for the lignite has an average value of 0.37 R_r% which comes under low rank B. However, some higher values (0.43) also suggest the probability of slight hydrocarbons generation. The distribution pattern of *n*–alkanes is utilised to describe the odd–even predominance (OEP) in terms of maturity, and the maturity of the sediment is determined based on the OEP values. Immature organic matter is indicated by OEP values greater than 1.4, while OEP values between 1.2 and 1.4 indicate low mature organic matter (Dong *et al.*, 2024). The OEP values of the studied samples show that the top sample (NM–1–31) has a value approximately equal to 1 which may be an indication of increased thermal maturity and the rest of the two samples have values greater than 1.4 indicating immature organic matter. However, it should also be noted that OEP may be governed by other factors also.

Neyveli Lignite–bearing sequence constitutes one of the largest deposits of the country holding enormously thick seams occurring over a large extend in the Cauvery Basin. Here in the present study, the geochemical studies provide additional information on the depositional regime, hydrological and redox conditions, climatic scenario existed during the deposition of the lignite seams. Further it provides information on the hydrocarbon source potential of these deposits. The significance of coralliferous sediments as a source for oil and gaseous hydrocarbons are established decades back (Wilkins & George, 2002). This has additional significance as this basin has been categorised as Category–I (Mukherjee *et al.*, 2024). The near–surface deposits are being mined at various blocks in the Neyveli region since few decades. However, there are

still large quantities of deposit buried beneath the sedimentary succession. Thus, the organic composition and characteristics of these deposits' further points to its significance as a source for unconventional hydrocarbons also.

CONCLUSION

The geochemical and petrographical study of Neyveli Lignite Mine–1 deposit has been performed to understand the nature of the organic matter, depositional regime and hydrocarbon source potential. Based on the observations on the studied samples, the conclusions obtained are as follows.

● The lignite deposit is originated by the deposition of terrestrially derived organic matter from wax–rich flora such as terrestrial higher plants and mangroves thrived in a warm and humid climatic condition.
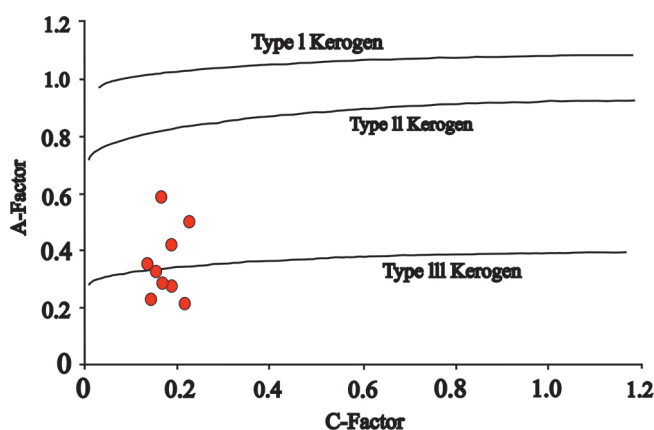

Fig. 10—Pseudo Van–Krevelen diagram of A–Factor vs. C–Factor obtained from FTIR spectra of the studied samples.
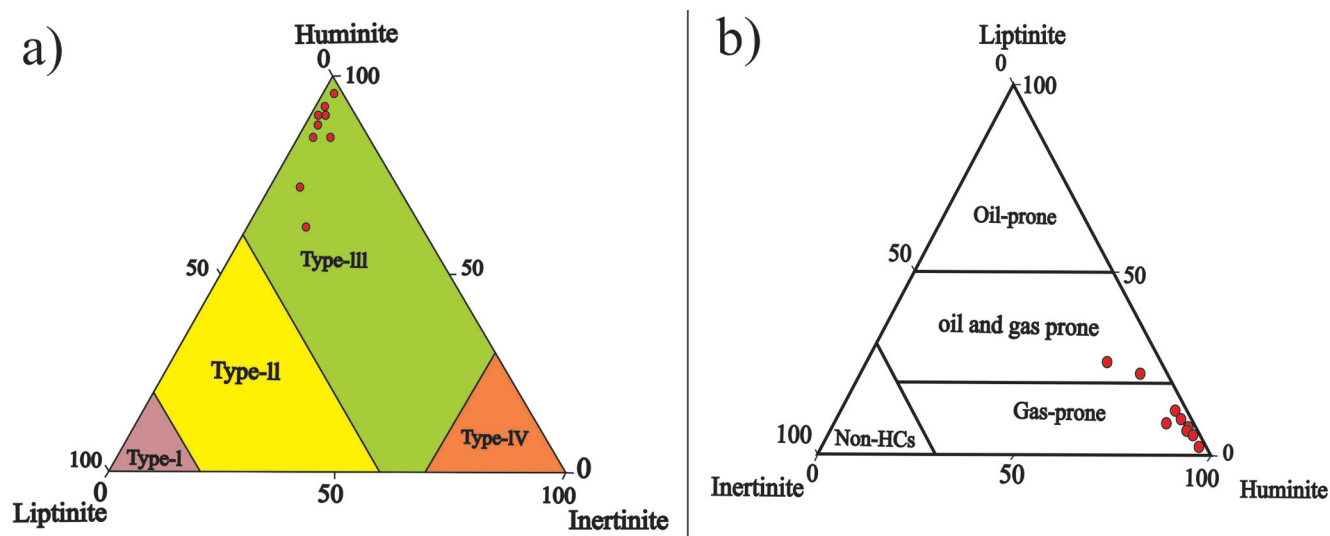
Fig. 11—Ternary diagrams illustrating (a) the kerogen type and (b) the nature of hydrocarbon based on the percentage of macerals.

- The peat precursors were deposited in a limno–telmatic depositional realm with mesotrophic to rheotrophic hydrological conditions. The transformation of these organic matters occurred generally under a suboxic conditions with increased microbial degradation of organic matter.

- The huminite reflectance range from 0.33 to 0.43% R_r in lignite suggests low rank–B, and immature nature of the samples. However, the presence of solid bitumen in the studied samples suggests some samples have neared maturity.

- The organic matter consists of type II/III mix kerogen, with substantial amount of liptinite macerals and perhydrous huminite, have the potential to generate gaseous hydrocarbons with some amount of oil upon maturity.

REFERENCES

Anandan KS, Sahay SN, Ramabadran TK & Prasad S 2010. Ground Water Control Technique for Safe Exploitation of the Neyveli Lignite Deposit, Cuddalore District, Tamil Nadu, India. Mine Water and the Environment 29: 3–13. https://doi.org/10.1007/s10230–009–0089–1.

Andersson RA, Kuhry P, Meyers P, Crill YZP & Mörth M 2011. Impacts of palaeohydrological changes on n–alkane biomarker compositions of a Holocene peat sequence in the eastern European Russian Arctic. Organic Geochemistry 42(9): 1065–1075. https://doi.org/10.1016/j.orggeochem.2011.06.020.

Bourbonniere RA & Meyers PA 1996. Sedimentary geolipid records of historical changes in the watersheds and productivities of Lakes Ontario and Erie. Limnology and Oceanography 41: 352–359. https://doi.org/10.4319/lo.1996.41.2.0352.

Calder JH, Gibbing MR & Mukhopadhyay PK 1991. Peat formation in a Westphalian B piedmont setting, Cumberland Basin, Nova Scotia: implication for the maceral–based interpretation of rheotrophic and raised paleomires. Société Géologique de France 162: 283–298.

Chakraborty C, Rana MS, Srivastava D, Giridhar MV & Mohan B 2010. Evolution of tectono–stratigraphic units and associated depositional system within syn–rift part in Nagapattinam sub basin, Cauvery Basin. 8th Bienneal International Conference & Exposition on Petroleum Geophysics.

Chari MVN, Sahu JN, Banerjee B, Zutshi PL & Chandra K 1995. Evolution of the Cauvery Basin, India from subsidence modelling. Marine and Petroleum Geology 12(6): 667–675. https://doi.org/10.1016/0264–8172(95)98091–I.

Diessel CFK 1992. Coal Bearing Depositional Systems. Springer–Verlag, Berlin: 721. https://doi.org/10.1007/978–3–642–75668–9.

Dong C, Wu J, Liu J, Zhang W, Grimay S, Fang P, Tao X, Zhu G & Han Y 2024. Even carbon number predominance observed in C50–C110 n–alkanes and monocyclic alkanes in the highly mature source rock. Fuel 355. https://doi.org/10.1016/j.fuel.2023.129360.

Eglinton G & Hamilton RJ 1967. Leaf epicuticular waxes. Science 156: 1322–1335. doi:10.1126/science.156.3780.1322

Ficken KJ, Li B, Swain DL & Eglinton G 2000. An n–alkane proxy for the sedimentary input of submerged/floating freshwater aquatic macrophytes. Organic Geochemistry 31: 745–749. https://doi.org/10.1016/S0146–6380(00)00081–4.

Ganz H & Kalkreuth W 1987. Application of infrared spectroscopy to the classification of kerogentypes and the evaluation of source rock and oil shale potentials. Fuel 66(5): 708–711. https://doi.org/10.1016/0016–2361(87)90285–7.

Ghosh S, Dutta S, Bhattacharyya S, Konar R & Priya T 2022. Paradigms of biomarker and PAH distributions in lower Gondwana bituminous coal lithotypes. International Journal of Coal Geology 260: 104067. https://doi.org/10.1016/j.coal.2022.104067.

Gola MR, Karger M, Gazda L & Grafka O 2013. Organic geochemistry of Upper Carboniferous bituminous coals and clastic sediments from the Lublin Coal Basin (Poland). Acta Geologica Polonica 63: 425–442.

Guo Y & Bustin RM 1998. Micro–FTIR spectroscopy of liptinite macerals in coal. International Journal of Coal Geology 36: 259–275. https://doi.org/10.1016/S0166–5162(97)00044–X

Hakimi MH, Kumar A, Singh AK, Lashin A, Rahim A, Varfolomeev MA, Yelwa NA & Mustapha KA 2023. Geochemistry and organic petrology of the bituminite shales from the Kapurdi mine, Rajasthan of NW India: implications for waxy oil generation potential. Journal of Petroleum Exploration and Production Technology 13: 505–521. https://doi.org/10.1007/s13202–022–01597–9.

He X, Liu X, Nie B & Song D 2017. FTIR and Raman spectroscopy characterisation of functional groups in various rank coals. Fuel 206: 555–563. https://doi.org/10.1016/j.fuel.2017.05.101

Hunt MJ 1995. Petroleum Geochemistry and Geology. W.H. Freeman and company, New York, USA, 743 pp.

ICCP 2001. The new inertinite classification (ICCP System 1994). Fuel 80(4): 459–471.

ISO 11760. "Classification of coals." International standard (2018).

ISO 7404–1, 2016. Methods for the Petrographic Analysis of Coals — Part 2: Vocabulary. International Organization for Standardization, Geneva, Switzerland.

ISO 7404–2, 2009. Methods for the Petrographic Analysis of Coals — Part 2: Methods of Preparing Coal Samples. International Organization for Standardization, Geneva, Switzerland. 12 pp.

ISO 7404–3, 2009. Methods for the Petrographic Analysis of Coals—Part 3: Method of Determining Maceral Group Composition. International Organization for Standardization, Geneva, Switzerland. 7 pp.

ISO 7404–5, 2009. Methods for the Petrographic Analysis of Coal—Part 5: Methods of Determining Microscopically the Reflectance of Vitrinite. International Organization for Standardization, Geneva, Switzerland. 14 pp.

Jones PH & Subramanyam V 1961. Ground–water control in the Neyveli Lignite field, South Arcot District, Madras State, India. Economic Geology 56(2): 273–298. doi: https://doi.org/10.2113/gsecongeo.56.2.273

Kalaitzidis S, Bouzinos A & Christanis K 2000. Paleoenvironment of lignite formation prior to and after the deposition of the "characterstic sand". The Lignite Deposit of Ptolemais 115: 29–42.

Kalaitzidis S, Bouzinos A, Papazisimou S & Christanis K 2004. A short–term establishment of forest fen habitat during Pliocene lignite formation in the Ptolemais Basin, NW Macedonia, Greece. International Journal of Coal Geology 57: 243–263. https://doi.org/10.1016/j.coal.2003.12.002.

Karadirek S 2023. Paleoenvironmental Settings of the Soma Coal Basin (Turkey): Insights from Maceral Data, Biomarker, and Carbon Isotopic Composition, ACS Omega 8 (50). https://doi.org/10.1021/acsomega.3c06635

Karthikeyan S, Kumar A, Peter AL, Divakar G & Johny A 2018. Study of Cauvery Basin, Damodar Valley Basin for Shale Oil and Gas. International Journal of Science Technology & Engineering 4(10): 58–65.

Khan R, Israili SH, Ahmad H & Mohan A 2005. Heavy metal pollution assessment in surface water bodies and its suitability for irrigation around the Neyevli Lignite Mines and associated industrial complex, Tamil Nadu, India. Mine Water Environment 24: 155–161. https://doi.org/10.1007/s10230–005–0087–x

Killops SD & Killops VJ 1993. An Introduction to Organic Geochemistry. 265 pp. Harlow: Longman: 265 pp.

Kumar D, Ghosh S, Tiwari B, Varma AK, Mathews RP & Chetia R 2021. Palaeocene–Eocene organic sedimentary archives of Bikaner–Nagaur Basin, Rajasthan, India: An integrated revelation from biogeochemical and elemental proxies. International Journal of Coal Geology 427. https://doi.org/10.1016/j.coal.2021.103848

Li Y, Chen S, Lu J, Wang G, Zou X, Xiao Z, Su K, He Q & Luo X 2020. The logging recognition of solid bitumen and its effect on physical properties, AC, resistivity and NMR parameters. Marine and Petroleum Geology 112: 104070. https://doi.org/10.1016/j.marpetgeo.2019.104070

Mallick M, Dutta S, Singh B, Bhattacharya S & Singh A 2021. Petrographic and organic geochemical characterisations of Early Eocene Lignites, Cambay Basin, western India. In: Bhui UK –Macromolecular characterisation of Hydrocarbons for sustainable future. Springer Green Energy and Technology: 143–171. https://doi.org/10.1007/978–981–33–6133–1_11.

Mastalerz M, Drobniak A & Stankiewicz AB 2018. Origin, properties and implications of solid bitumen in source–rock reservoirs: A review, International Journal of Coal Geology 195: 14–36. https://doi.org/10.1016/j.coal.2018.05.013.

Mathews RP, Singh BD, Singh VP, Singh A, Singh H, Shivanna M, Dutta S, Mendhe VA & Chetia R 2020. Organo–petrographic and geochemical characteristics of Gurha Lignite deposits, Rajasthan, India: Insights into the palaeovegetation, palaeoenvironment and hydrocarbon source rock potential. Geoscience Frontiers 11(3): 965–988. https://doi.org/10.1016/j.gsf.2019.10.002.

Matthewman R, Martins Z & Sephton M 2013. Type IV Kerogens as analogues for organic macromolecular materials in aqueously altered carbonaceous chondrites. Astrobiology 13: 324–333. https://doi.org/10.1089/ast.2012.082.

Misra BK 1992. Genesis of Indian Tertiary coals and lignites–a biopetrological and palaeobotanical view point. Palaeobotanist 40: 490–513.

Mukherjee S, Ansari K, Raha A, Biswas M & Mazumder S 2024. Tectonics of Cauvery Basin (India) in onshore and offshore portions. Marine and Petroleum Geology, p.107142. https://doi.org/10.1016/j.marpetgeo.2024.107142.

Mukhopadhyay PK 1986. Petrography of selected Wilcox and Jockson Group lignites from Tertiary of Texas. Geology of Gulf Coast Lignites. Geological Society of America Coal Geology Division Field Trip Guidebook, Environmental and Coal Associates, Houston, Texas 202: 126–145.

Nagendra R & Reddy AN 2017. Major geologic events of the Cauvery Basin, India and their correlation with global signatures–A review. Journal of Palaeogeography 6(1): 69–83. https://doi.org/10.1016/j.jop.2016.09.002.

Navale GKB 1967. Microfossil analysis of Neyveli Lignite by polished surface technique. Palaeobotanist 16: 141–144.

Navale GKB & Misra BK 1980. Systematic study of the organic microconstituents of the main seam of Neyveli Lignite, South India. Geophytology 10: 245–264.

Periyasamy N 2019. Geotechnical and Hydrological Challenges in Neyveli Lignite Mines, Tamil Nadu. Journal of Geological Society of India 94(3): 334–334. https://doi.org/10.1007/s12594–019–1315–5.

Peters KE, Walters CC & Moldowan JM 2005. The Biomarker Guide. 2nd Edition Cambridge University Press, New York. https://doi.org/10.1017/CBO9780511524868.

Pickel W, Kus J, Flores D, Kalaitzidis S, Christanis K, Cardott BJ, Misz Kennan M, Rodrigues S, Hentschel A, Hamor–Vido M, Crosdale P & Wagner N 2017. Classification of liptinite–ICCP System 1994. International Journal of Coal Geology 169: 40–61. https://doi.org/10.1016/j.coal.2016.11.004.

Pranesh V, Balasubramanian S, Kumar RS, Sakthivel R, Rajkumar P & Ravikumar S 2019. Kaolinite flakes and coal fines production in Lignite Core under ambient conditions: A case study of Neyveli Lignite field at Cauvery Basin, Southern India. Journal of Natural Gas Science and Engineering 64: 72–80. https://doi.org/10.1016/j.jngse.2019.01.023.

Premarathne U 2015. Petroleum Potential of the Cauvery Basin, Sri Lanka: A Review. Journal of Geological Society of Sri Lanka 17: 41–52.

Ramkumar M, Menier D, Mathew M, Santosh M & Siddiqui N 2017. Early Cenozoic rapid flight enigma of the Indian subcontinent resolved: Roles of topographic top loading and subcrustal erosion. Geoscience Frontiers 8(1): 15–23. https://doi.org/10.1016/j.gsf.2016.05.004.

Ramkumar M, Stüben D & Berner Z 2011. Barremian–Danian chemostratigraphic sequences of the Cauvery Basin, India: Implications on scales of stratigraphic correlation. Gondwana Research 19: 291–309. 10.1016/j.gr.2010.05.014.

Sastri VV, Sinha RN, Singh G & Murti KVS 1973. Stratigraphy and tectonics of sedimentary basins on East Coast of Peninsular India. AAPG Bulletin 57(4): 655–678. https://doi.org/10.1306/819A4312–16C5–11D7–8645000102C1865D

Saxena RK 1992. Neyveli Lignites and associated sediments–their palynology, palaeoecology, correlation and age. Palaeobotanist 40: 345–353.

Scalan RS & Smith JE 1970. An improved measure of odd–even predominance in normal alkanes of sediment extracts and petroleum. Geochimica et Cosmochimica Acta 34(5): 611–620. https://doi.org/10.1016/0016–7037(70)90019–0.

Sen D, Ghosh S & Varma AK 2022. Functional group chemistry and its functions in coal carbonization: a scientific intelligence from infrared spectroscopy. Arabian Journal of Geosciences 15(5): 406. https://doi.org/10.1007/s12517–022–09719–7.

Singh A & Misra BK 1999. Fluorescence microscopic investigations of the main lignite seam from the Neyveli Lignite field, Tamil Nadu, India. Palaeobotanist 48(2): 155–162.

Singh A & Singh BD 1994. Reflectance measurements on maturation of the Neyveli Tertiary brown coals (lignites), south India. Minetech 14(3): 13–22.

Singh A, Misra BK, Singh BD & Navale GKB 1992. The Neyveli Lignite deposits (Cauvery Basin), India: organic composition, age and depositional pattern. International Journal of Coal Geology 21: 45–97. https://doi.org/10.1016/0166–5162(92)90035–U.

Singh PK, Singh MP, Singh AK & Mukesh A 2010a. Petrographic characteristics of coal from the Lati Formation, Tarakan Basin, East Kalimantan, Indonesia. International Journal of Coal Geology 81(2): 109–116. https://doi.org/10.1016/j.coal.2009.11.006.

Singh VP, Singh BD, Mathews RP, Mendhe VA, Agnihotri P, Mishra S, Radhwani M, Dutta S, Subramanian KA, Singh A & Singh H 2021. Petrographical–geochemical characteristics and floral–faunal compositions of the Valia Lignite deposits from Cambay Basin (Gujarat), western India. International Journal of Coal Geology 248. https://doi.org/10.1016/j.coal.2021.103866

Singh VP, Singh BD, Mathews RP, Singh A, Mendhe VA, Mishra S & Bannerjee M 2022. Palaeodepositional and Hydrocarbon Source–Rock characteristics of the Sonari Succession (Paleocene), Barmer Basin, NW India: Implications from Petrography and Geochemistry. Natural Resources Research 31: 2943–2971. https://doi.org/10.1007/s11053–022–10079–y

Singh VP, Singh BD, Mathews RP, Singh A, Mendhe VA, Singh PK, Mishra S, Dutta S, Shivanna M & Singh MP 2017. Investigation on the lignite deposits of Surkha Mine (Saurashtra Basin, Gujarat), western India: Their depositional history and hydrocarbon generation potential. International Journal of Coal Geology 183: 78–99. https://doi.org/10.1016/j.coal.2017.09.016.

Singh VP, Singh BD, Singh A, Singh MP, Mathews RP, Dutta S, Mendhe VA, Mahesh S & Mishra S 2017. Depositional palaeoenvironment and economic potential of Khadsaliya Lignite deposits (Saurashtra Basin), western India: Based on petrographic, palynofacies and geochemical characteristics. International Journal of Coal Geology 171: 223–242 https://doi.org/10.1016/j.coal.2017.01.007

Sýkorová I, Pickel W, Christanis K, Wolf M, Taylor & Flores D 2005. Classification of huminite—ICCP System 1994. International Journal of Coal Geology 62(1–2): 85–106. https://doi.org/10.1016/j.coal.2004.06.006.

Watkinson M, Hart MB & Joshi A 2007. Cretaceous tectonostratigraphy and the development of the Cauvery Basin, southeast India. Petroleum Geoscience 13(2): 181–191.

Wilkins RW & George SC 2002. Coal as a source rock for oil: a review. International Journal of Coal Geology 50(1–4): 317–361. https:// doi.org/10.1016/S0166–5162(02)00134–9

Zheng Y, Zhou W, Meyers PA & Xie S 2007. Lipid biomarkers in the Zoige–Hongyuan peat deposit: indicators of Holocene climate changes in West China. Organic Geochemistry 38: 1927–1940. https://doi.org/10.1016/j.orggeochem.2007.06.012

Životić D, Jovančićević B, Schwarzbauer J, Cvetković O, Gržetić I, Ercegovac M, Stojanović K & Šajnović A 2010. The petrographical and organic geochemical composition of coal from the East field, Bogovina Basin (Serbia). International Journal of Coal Geology 81(4): 227–241. https://doi.org/10.1016/j.coal.2009.07.012.